Probing 29Si-17O connectivities and proximities by solid-state NMR

Frédérique Pourpoint, Florian Venel, Raynald Giovine, Julien Trébosc, Tom Vancompernolle, Mostafa Taoufik, Vincent Sarou-Kanian, Régis Gauvin, Olivier Lafon

Probing ^{29}Si-^{17}O connectivities and proximities by solid-state NMR

Frédérique Pourpoint*[a], Florian Venel[a], Raynald Giovine[a], Julien Trébosc[a], Tom Vancompernolle[a], Mostafa Taoufik[b], Vincent Sarou-Kanian[c], Régis M. Gauvin[d], Olivier Lafon[a, e]

a. Univ. Lille, CNRS, Centrale Lille, Univ. Artois, UMR 8181–UCCS– Unité de Catalyse et Chimie du Solide, F-59000 Lille, France.

b. Université Lyon 1, Institut de Chimie de Lyon; CPE Lyon; CNRS, UMR 5265 C2P2, LCOMS; Bâtiment 308 F 43 Blvd du 11 Novembre 1918 F-69616, Villeurbanne Cedex, France.

c. CEMHTI, CNRS, UPR 3079, 1D avenue de la Recherche Scientifique, 45071 Orléans Cedex 2, France

d. PSL Research University, Chimie ParisTech - CNRS, Institut de Recherche de Chimie Paris, 75005, Paris, France

e. Institut Universitaire de France

Corresponding author: frederique.pourpoint@centralelille.fr

Abstract:

The measurement of dipolar and *J*- couplings between ^{29}Si and ^{17}O isotopes is challenging owing to (i) the low abundance of both isotopes and (ii) their close Larmor frequencies, which only differ by 19%. These issues are circumvented here by the use of isotopic enrichment and dedicated triple-resonance magic-angle spinning NMR probe. The surface of ^{29}Si-enriched silica was labelled with ^{17}O isotope and heated at 80 and 200 °C. ^{29}Si-^{17}O connectivities and proximities were probed using two-dimensional (2D) through-bond and through-space heteronuclear multiple-quantum coherences (*J*- and *D*-HMQC) experiments between ^{17}O and ^{29}Si nuclei. The simulation of the build-up of the *J*- and *D*-HMQC signals allowed the first experimental measurement of *J*- and dipolar coupling constants between ^{17}O and ^{29}Si nuclei. These HMQC experiments allow distinguishing two distinct siloxane (SiOSi) oxygen sites: (i) those covalently bonded to Q^3 and Q^4 groups, having a hydroxyl group as a second neighbour and (ii) those covalently bonded to two Q^4 groups. The measured *J*- and dipolar coupling constants of siloxane ^{17}O nucleus with Q^4 ^{29}Si nuclei differ from those with Q^3 ^{29}Si nuclei. These results indicate that the ^{29}Si-^{17}O one-bond *J*-coupling and Si-O bond length depend on the second neighbours of the Si atoms.

Introduction:

The design and understanding of catalytic materials critically depend on efficient spectroscopic methods, in order to determine structure-activity relationships. Among the available characterisation techniques, solid-state NMR holds a prominent position, as it provides structural information down to the molecular level, even for sites lacking long-range positional order[1-3]. Solid-state NMR spectroscopy allows probing the local environment of a nucleus, not only by measuring its chemical shift and its quadrupolar coupling, but also by observing connectivities and proximities through *J*- and dipolar couplings[4, 5]. When relating this to catalytic materials, this powerful approach allows to draw a reliable picture on the nature and topology of the sites relevant to specific reactivity. More specifically, in the case of silica, a class of material that is used on a huge scale both as catalyst or as catalytic support, NMR techniques have been proved to be essential for the precise characterization of their surface and of the active sites within SiO_2-supported catalysts[1, 6, 7]. Moreover, the silica exhibits different local surface environments, as a result from water elimination stemming from silanol condensation (Scheme 1). Whereas ^{1}H, ^{29}Si and ^{17}O NMR and first-principles calculations are commonly used to probe the local structure of the silica[8-13], ^{17}O-^{29}Si heteronuclear correlation and the measurement of *J*- and dipolar couplings between these isotopes remain a great challenge. The interest in its overcoming is substantial: such correlation would provide bond and/or distance information mandatory for the precise description of the silica structure, which would be a first step for the refined understanding of silica-supported catalysts.

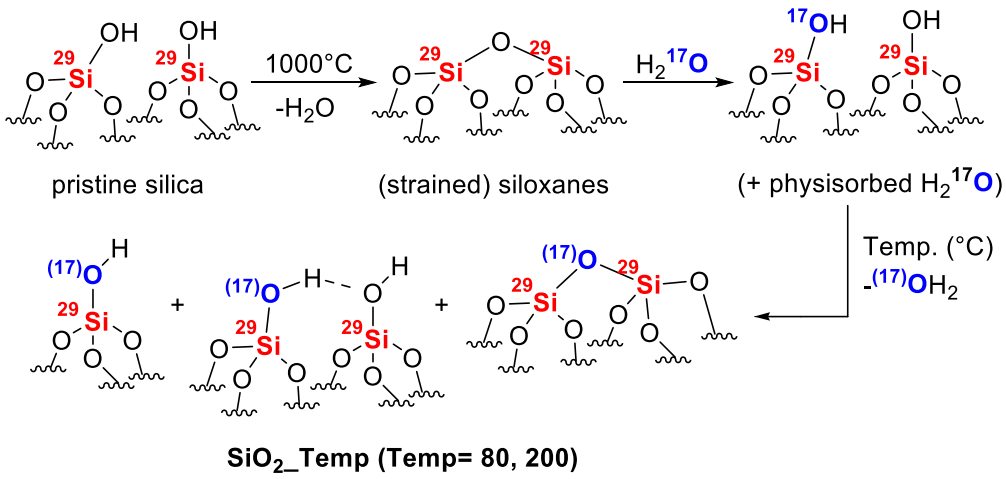

Scheme 1: Synthesis of doubly labelled silica.

J-couplings provide unique information about the chemical bonds. They are widely used for the structural characterization of molecules in liquids[14, 15], since the splitting due this interaction is often directly observed on the 1D spectra. The *J*-coupling splitting can also be directly observed on the spectra of highly mobile solids, such as plastic crystals[16, 17]. Conversely, in rigid solids, the *J*-coupling splittings are often masked by anisotropic interactions, such as dipolar interactions, chemical shift anisotropy or quadrupolar interaction for nuclear spin $I \geq 1$, as well as the distribution of isotropic chemical shifts due

to atomic-level disorders. Nevertheless, two-dimensional (2D) NMR experiments have been developed to observe and measure *J*-coupling in solids, including:

(i) homonuclear *J*-coupling between spin-1/2 nuclei (^{31}P-^{31}P[18], ^{29}Si-^{29}Si,[19] ^{13}C-^{13}C[20] and ^{15}N-^{15}N[21]) or between quadrupolar nuclei (^{11}B-^{11}B[22] and ^{71}Ga-^{71}Ga[23]),

(ii) heteronuclear *J*-couplings between spin-1/2 nuclei (^{31}P-^{29}Si[24], ^{31}P-^{113}Cd[24], ^{31}P-^{77}Se[24], ^{1}H-^{13}C[25]) or between spin-1/2 and half-integer quadrupolar isotopes (^{27}Al-^{31}P[26], ^{27}Al-^{29}Si[26], ^{31}P-^{71}Ga[27], ^{77}Se-^{71}Ga[28], ^{13}C-^{17}O, ^{15}N-^{17}O[29], ^{1}H-^{17}O[30], ^{27}Al-^{17}O[31]).

Nevertheless, to the best of our knowledge, ^{17}O-^{29}Si *J*- and dipolar couplings have never been measured. One-bond ^{17}O-^{29}Si ^{1}J-coupling constants have so far only been calculated using density functional theory (DFT) in SiP_2O_7 polymorphs[32]. The only example of 2D ^{17}O-^{29}Si correlation spectrum reported in the literature is a 2D ^{17}O-detected through-space heteronuclear multiple-quantum correlation (*D*-HMQC) spectrum of doubly ^{17}O and ^{29}Si-enriched germanosilicate zeolites, for which coherence transfer relies on ^{17}O-^{29}Si dipolar coupling[33]. The main limitation to measure ^{17}O-^{29}Si couplings is the low natural abundance (*NA*) of these isotopes: *NA*(^{29}Si) = 4.68%, and *NA*(^{17}O) = 0.037%. Furthermore, as the ^{17}O and ^{29}Si Larmor frequencies only differ by 19%, a specific triple-resonance magic-angle spinning (MAS) NMR probe is required, for which the X and Y channels can be tuned to these close resonance frequencies.

We show here how the connectivities and proximities between ^{17}O and ^{29}Si nuclei can be probed by measuring ^{17}O-^{29}Si *J*- and dipolar couplings. We also report the first 2D ^{17}O-^{29}Si through-bond HMQC (*J*-HMQC) spectrum. The experimental data are obtained on a ^{29}Si-enriched silica with surface enriched in ^{17}O.

Experimental Section

Sample preparation.

The samples were prepared in an argon-filled glove box, and materials were handled under inert atmosphere using standard Schlenk techniques. Samples of ^{29}Si-labelled silica (with ^{29}Si enrichment level of 100%) and ^{17}O-enriched water (with ^{17}O enrichment level of 70%) were purchased from Cortecnet. The ^{29}Si-labelled (0.5 g) silica was treated at 1000 °C under high vacuum (10^{-5} Torr) for 15 h, using a quartz tube reactor inserted in a tube furnace while connected to a high vacuum line. ^{17}O-enriched water (0.1 g, ^{17}O content 70%) was introduced in the reactor and left to react at room temperature for 8 h[34]. The material was then submitted to heat treatment under high vacuum for 15 h at the desired temperature (80 or 200°C), using the same experimental setup as for the first annealing step. The corresponding samples are denoted $SiO_{2\text{-}80}$ and $SiO_{2\text{-}200}$ hereafter.

NMR experiments

1D Hahn echo and 2D MQ-MAS NMR experiments were recorded at 18.8 T using a double-resonance (HX) 3.2 mm MAS NMR probe, spinning at 20 kHz at the NMR facility of the Advanced Characterization Platform of the Chevreul Institute located in Lille. Other NMR experiments were recorded at 20 T using a triple-resonance (HXY) 3.2 mm MAS NMR probe, spinning at 20 kHz at CEMHTI located in Orléans. The

1D ^{1}H, ^{17}O and ^{29}Si NMR spectra of Figs. **1** were acquired using Hahn-echo experiments for ^{1}H and ^{17}O isotopes and one-pulse experiment for ^{29}Si nucleus. The radiofrequency (RF) nutation frequencies were equal to 90 and 45 kHz for ^{1}H and ^{29}Si respectively. We used a central transition (CT)-selective pulse lasting 10 μs and a RF amplitude of 8 kHz for the ^{17}O NMR experiment. The 1D ^{1}H, ^{29}Si and ^{17}O NMR spectra of Figs. **1** result from averaging 32, 368 and 1024 transients, respectively, with recycle delays of 1, 5 and 0.5 s. 2D ^{17}O triple-quantum (3Q)-MAS NMR spectrum of $SiO_{2\text{-}200}$ was acquired using the three-pulse z-filter pulse sequence[35]. The 2D 3QMAS spectrum was sheared with the xfshear program included in the TOPSPIN software. We used excitation and reconversion pulses lasting t_p = 3.9 and 1.3 μs, respectively, with ν_1 = 64 kHz and a CT selective π/2 last pulse lasting 15.2 μs with ν_1 = 5 kHz. The T_2' time constant for the ^{17}O transverse losses, which cannot be refocused by a π pulse, was measured using Hahn echo experiment, in which the CT-selective π pulse with ν_1 = 8 kHz was bracketed by two rotor-synchronized delays. The Hahn echo spectra result from averaging 2560 transients with a recycle delay τ_{RD} = 0.5 s. We recorded ^{17}O{^{29}Si} *J* and *D*-HMQC experiments enhanced by double-frequency sweep (DFS[36]) and quadrupolar Carr-Purcell Meiboom-Gill (QCPMG)[37] as well as 2D double-quantum (2Q)-filtered DFS-*D*-HMQC-QCPMG spectra. For those experiments, we used equal defocusing and refocusing delays. Before the acquisition of *J*-HMQC data, the magic angle was carefully adjusted by maximizing the intensity of the spinning sidebands in the ^{2}H spectrum of deuterated hexamethylbenzene (HMB) in order to minimize the residual ^{29}Si-^{17}O dipolar couplings. This leads to an estimated accuracy of the magic angle of 0.01°[30, 38]. The DFS pulse lasted 2 ms and used ν_1 = 8 kHz. During the DFS pulse, the frequencies of the RF spikelets were linearly swept in a symmetric manner from 800 to 100 kHz with respect to the CT. The RF field strength of the central transition selective pulses on ^{17}O channel is 8 kHz, while the RF nutation frequency of the ^{29}Si π/2 pulse is 48 kHz. A continuous wave ^{1}H decoupling with ν_1 = 100 kHz was applied during the whole pulse sequence. For *D*-HMQC experiment, $\mathrm{SR4}_1^2$ recoupling with ν_1 = 40 kHz was applied on the ^{29}Si channel. During QCPMG acquisition, the delay between successive CT-selective π pulses was 1.4 ms and 50 echoes were acquired in every transient. Note that no enhancement of Si-^{17}OH signal was detected when applying ^{1}H decoupling during the QCPMG scheme, indicating that the T_2' constant is not limited by the ^{1}H-^{17}O dipolar couplings but is governed by the modulation of the ^{17}O quadrupolar interaction due to librational motion of the silanol groups[39]. We also acquired 1D ^{1}H→^{17}O through-space refocused INEPT (*D*-RINEPT) spectrum of $SiO_{2\text{-}200}$ at ν_R = 18 kHz. For this experiment, the RF-field of the pulses, which do not belong to the recoupling scheme, was equal to 100 kHz on ^{1}H channel and 8 kHz on ^{17}O channel. The ^{1}H-^{17}O dipolar couplings were reintroduced by applying $\mathrm{SR4}_1^2$ recoupling with ν_1 = 36 kHz on ^{1}H channel. ^{1}H and ^{29}Si isotropic chemical shifts were referenced to the resonance of neat tetramethylsilane (TMS) at δ_{iso} = 0 ppm, whereas the ^{17}O isotropic chemical shifts were referenced to water at δ_{iso} = 0 ppm. Additional experimental details are given in the figure captions.

Numerical simulations

Simulations were performed with SIMPSON software[40]. The powder average was calculated using 1512 different orientations between the molecular and rotor frames: 168 $\{\alpha_{MR}, \beta_{MR}\} \times 9\ \gamma_{MR}$ angles. The {α_{MR},

β_{MR}} Euler angles were selected according to the REPULSION algorithm[41], while the γ_{MR} angle was equally stepped from 0 to 360°. The simulations were carried out for an isolated ^{29}Si-^{17}O^{29}Si spin system. The ^{17}O quadrupolar coupling constant and the asymmetry parameter of the electric field gradient were fixed to 5.4 MHz and 0.32, respectively, which correspond the best-fit NMR parameters to simulate ^{17}O signal of siloxane group in MQMAS spectrum (Fig. S1). A ^{17}O CSA of 50 ppm[42, 43], *J* anisotropy and ^{29}Si-^{29}Si *J*- and dipolar coupling were considered. The two ^{29}Si nuclei were located in the XZ plane of the principal axis system of the ^{17}O electric field gradient (efg) tensor. As explained below, the Si-O-Si angle and the Si-O distances were varied. We simulated the ^{17}O{^{29}Si} *D*-HMQC experiments. All pulses were applied on resonance. Other simulation parameters were identical to the reported experimental values.

Results and discussion

Building on our previous experience with selectively surface-enriched silica,[34] this sample was synthesized, using commercial ^{29}Si-labelled SiO_2 and ^{17}O-enriched H_2O (see experimental section). In a first stage, the heating of the silica under vacuum at 1000 °C during 15 h provided a highly hygroscopic material, which was then reacted with ^{17}O-labelled water, yielding Si-O-Si and Si-OH centres. Further treatment of the resulting material at 80 or 200 °C temperature leads to the samples of interest $SiO_{2\text{-}80}$ and $SiO_{2\text{-}200}$, respectively (Scheme **1**), which are enriched in ^{29}Si in the whole particle volume and in ^{17}O near or on the surface. These treatment temperatures were chosen 1) to avoid extensive dehydroxylation, which would deplete ^{17}O content and 2) to limit the extent of ^{17}O oxygen migration into the bulk of the material so that only surface sites are enriched with ^{17}O.[34] Furthermore, these intermediate temperatures allow the removal of (most of) physisorbed H_2O, while avoiding a complete condensation of silanols (Si-OH) into siloxane moieties (Si-O-Si).

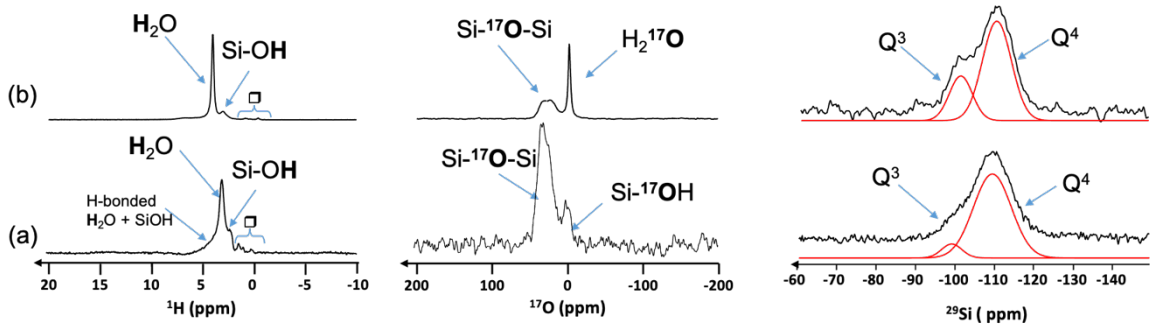

Figure 1. 1D ^{1}H, ^{17}O and ^{29}Si NMR spectra recorded at 18.8 T with a MAS frequency ν_R = 20 kHz of (a) $SiO_{2\text{-}200}$ and of (b) $SiO_{2\text{-}80}$. The ❐ denotes an impurity. The red spectra are the simulations obtained with DMFit software[44].

The 1D ^{1}H, ^{17}O and ^{29}Si NMR spectra of $SiO_{2\text{-}200}$ are displayed in Fig. 1a. The ^{1}H NMR spectrum exhibits characteristic signals at 3.5 and 2.1 ppm, assigned to physisorbed water and isolated Si-OH groups, respectively as well as a deshielded shoulder ascribed to hydrogen-bonded SiOH[45, 46]. The ^{29}Si spectrum consists of two overlapping signals of $Si(OSi)_n(OH)_{4-n}$ with n = 3 and 4 (denoted Q^3 and Q^4)[47]. The relative amount obtained with the deconvolution of these sites is 15% for the Q^3 and 85% for the Q^4. The ^{17}O

spectrum displays a broad signal centered at 28 ppm corresponding to Si-^{17}O-Si moieties as well as a lower intensity peak at 0 ppm ascribed to Si-^{17}OH [34, 48]. We also recorded 2D ^{17}O 3Q-MAS spectrum (see Fig. **S1**) where two signals are clearly separated. The signal with δ_{iso} = 40 ppm, C_Q = 5.4 MHz and η_Q = 0.32 is assigned to siloxane Si-^{17}O-Si environment, while the signal resonating at 25 ppm is attributed to an impurity. However, its relative amount is approximately equal to 5%. The lack of silanol Si-^{17}O-H environment in the 2D 3Q-MAS spectrum stems most probably from its small C_Q value[49] and low relative amount compared to the Si-^{17}O-Si site[34]. The 1D ^{1}H, ^{17}O and ^{29}Si NMR spectra of $SiO_{2\text{-}80}$ are displayed in Fig. 1b. The ^{1}H and ^{17}O NMR spectra of this sample exhibit a more intense signal of physisorbed water, in agreement with the lower temperature of the thermal treatment, whereas its ^{29}Si NMR spectrum is similar to that of $SiO_{2\text{-}200}$, with a greater relative amount of Q^3 (26% of Q^3 and 74% of Q^4).

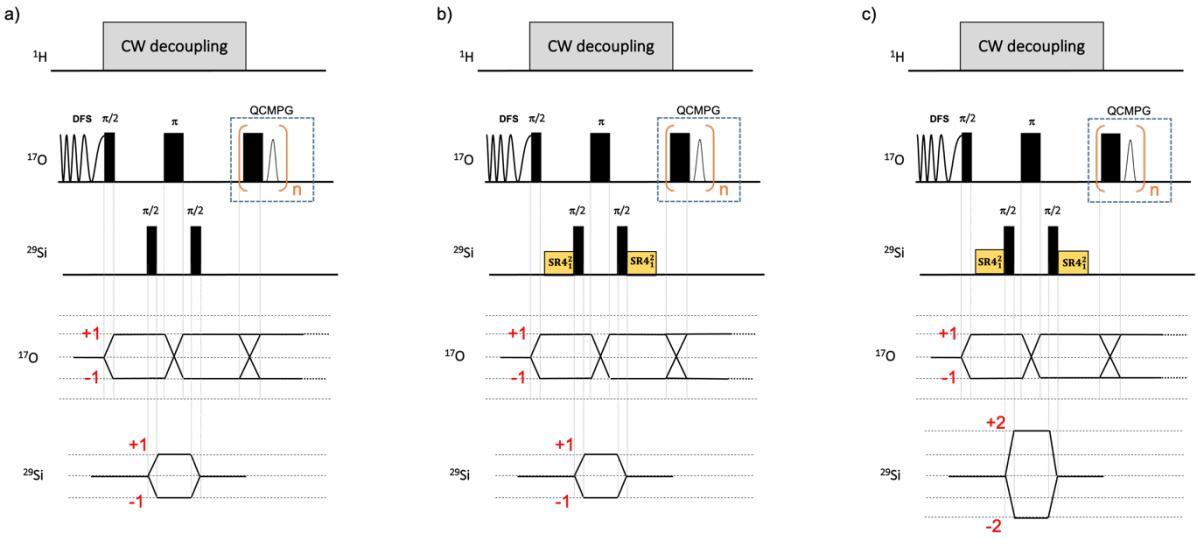

Figure 2. ^{17}O-{^{29}Si} DFS-HMQC-QCPMG pulse sequences using coherence transfers via ^{17}O-^{29}Si (a) *J*- or (b,c) dipolar coupling. The coherence transfer pathways for ^{17}O and ^{29}Si channels are shown at the bottom of the figure. For the *D*-HMQC sequences, we selected via phase cycling either (b) single-quantum (SQ) and (c) 2Q ^{29}Si coherences during the indirect evolution period, t_1. The pulse programs of pulse sequences (b) and (c) are given in the Appendix 2 of the Supporting Information.

To gain further insights into the connectivities and proximities between ^{17}O and ^{29}Si isotopes, we recorded 2D ^{17}O-^{29}Si heteronuclear correlation. ^{17}O excitation was employed since it is more sensitive than ^{29}Si excitation because ^{17}O longitudinal relaxation times are much shorter than those of ^{29}Si nuclei $T_1(^{17}\mathrm{O}) \ll T_1(^{29}\mathrm{Si})$[50-52]. Besides, ^{17}O detection was preferred since in the investigated sample, only the surface sites are enriched in ^{17}O and a significant fraction of ^{29}Si nuclei are not bonded to ^{17}O and can produce t_1-noise in 2D ^{17}O-^{29}Si heteronuclear correlation spectra using ^{29}Si detection. Therefore, ^{17}O and ^{29}Si signals were correlated using *J* and *D*-HMQC spectra with ^{17}O excitation and the indirect detection of ^{29}Si nuclei (^{17}O{^{29}Si}). Furthermore, the signal was enhanced using the DFS[36], which increases the polarization of the CT by manipulating the population of the satellite transitions (ST). In addition, the T_2' time constant is equal to 65 ms for siloxane ^{17}O nuclei. Hence, their signal was enhanced by using the

QCPMG detection, which allowed the acquisition of 50 echoes in every transient. The corresponding sequence is displayed in Fig. **2**. 2D $^{17}O\{^{29}Si\}$ DFS-*J* and *D*-HMQC-QCPMG spectra of $SiO_{2\text{-}200}$ are shown in Figs. **3**. The *D*-HMQC-QCPMG spectrum exhibits two cross peaks in the Si-O-Si region attributed to the ^{17}O nuclei close to $^{29}Si(Q^3)$ and $^{29}Si(Q^4)$ environments.[47] The lack of Si-^{17}OH signal stems from (1) the small amount of Si-^{17}OH as compared to the Si-^{17}O-Si groups and (2) their short T_2' time constant equal to 9 ms, which reduces the efficiency of the coherence transfer and the signal enhancement by QCPMG scheme.

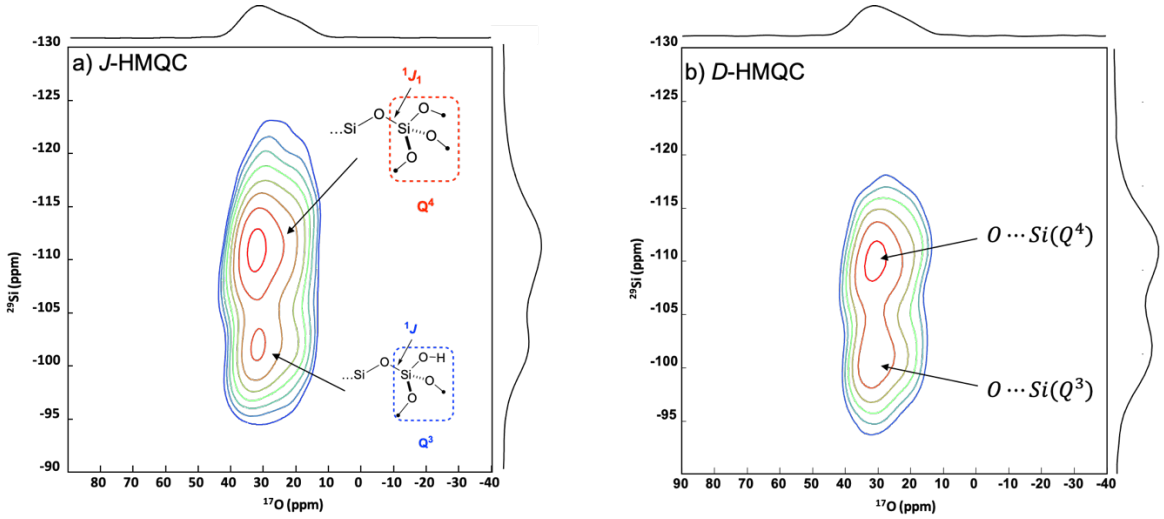

Figure 3. 2D $^{17}O\{^{29}Si\}$ DFS-(a) *J*- and (b) *D*-HMQC-QCPMG NMR spectrum of $SiO_{2\text{-}200}$ recorded at 20 T with ν_R = 20 kHz (a) The *J*-HMQC spectrum was recorded with τ = 10 ms, 14848 transients for each of 24 t_1 increments with a recycle delay τ_{RD} = 0.5 s, leading to an experimental time of 50 h (b) The *D*-HMQC spectrum was recorded with τ = 3 ms ms (recoupling time), 5120 transients for each of 22 t_1 increments with a recycle delay τ_{RD} = 0.5 s, leading to an experimental time of 16 h The projections along ^{29}Si and ^{17}O dimensions are also shown.

The $^{17}O\{^{29}Si\}$ *J*-HMQC-QCPMG spectrum shown in Fig. **3a** exhibits the same cross peaks as the *D*-HMQC spectrum (Fig. **3b**). These cross-peaks represent the first experimental observation of ^{17}O-^{29}Si *J*-couplings. For the sake of comparison, ^{17}O-$\{^{29}Si\}$ *J*- and *D*-HMQC spectra of $SiO_{2\text{-}80}$ were also recorded (see Fig. **S3**) and also display O-Si(Q^3) and O-Si(Q^4) cross-peaks, and no cross-peak for Si-OH. The lack of cross-peak at $\delta(^{17}O)$ = 0 ppm is consistent with its assignment to water (Fig. **1b**).

In order to measure ^{17}O-^{29}Si *J*-couplings, we recorded 1D $^{17}O\{^{29}Si\}$ DFS-*J*-HMQC-QCPMG spectra with various defocusing and refocusing delays, τ (see Fig. **S2**). During these delays, the single-quantum coherences associated to the ^{17}O CT evolve under the ^{17}O-^{29}Si *J*-couplings. However, these delays are not affected by the dipolar-quadrupolar cross-term since the Hamiltonian of this term is proportional to $[3I_z^2 - I(I+1)\mathbf{1}_I]S_z$,[53 54] which commutes with the operators associated to the ^{17}O CT. In the expression of the above product of spin operators, I = 5/2 is the spin value of ^{17}O, I_z and S_z denote the operators associated to the *z*-component of the spin angular momentum of ^{17}O and ^{29}Si nuclei, respectively, and $\mathbf{1}_I$ is the identity matrix of size 2I+1. Furthermore, the magic angle was adjusted with an accuracy better than 0.05°, which results in residual ^{17}O-^{29}Si dipolar couplings smaller than $\pm$1 Hz.

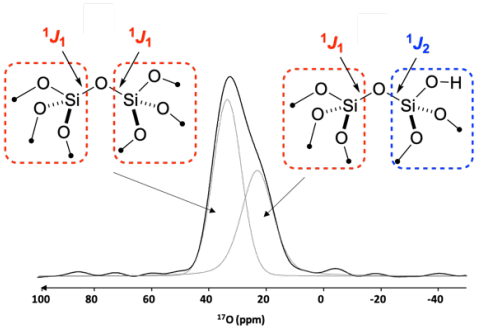

Fig. 4. 1D ^{17}O-{^{29}Si} DFS-*J*-HMQC-QCPMG NMR spectra of $SiO_{2\text{-}200}$ recorded with τ = 9 ms. Experimental parameters are given in the caption of the Figure 5.

As seen in Figs. **S2** and **4**, 1D ^{17}O{^{29}Si} DFS-*J*-HMQC-QCPMG spectra exhibit a peak at 34 ppm as well as a shoulder at 22 ppm. These two signals are barely resolved in the 3Q-MAS spectrum of Fig. **S1**. However, the build-up curves at these two shifts differ, as seen in Fig. **5b** and **c**. The maximal intensity is reached at τ = 7 ms for the deshielded site, instead of 9 ms for the shielded signal. These distinct build-up curves suggest the presence of at least two distinct ^{17}O sites subject to different ^{17}O-^{29}Si *J*-couplings. Furthermore, the intensity of the deshielded signal is always higher than that of the shielded one (Fig. **S2**). Based on this difference in intensity, the deshielded and shielded sites were assigned to symmetrical (Si(Q^4)-O-Si(Q^4)) and asymmetrical (Si(Q^3)-O-Si(Q^4)) siloxane environments, respectively (see Fig. **5a**), since the amount of Q^3 sites near the silica surface is known to be lower than that of Q^4 sites. Given the amount of hydroxyl groups near the surface of $SiO_{2\text{-}200}$, the contribution of Si(Q^3)-O-Si(Q^3) sites to the *J*-HMQC build-up curves has been neglected. For the symmetrical environment (scheme **A** in Fig. **5a**), one-bond ^{17}O-^{29}Si *J*-couplings were assumed to be equal and the transfer efficiency of ^{17}O-{^{29}Si} *J*-HMQC experiment is proportional to

$$2A[\sin^2(\pi J_1\tau)\cos^2(\pi J_1\tau)]\left[\exp\left(-\frac{2\tau}{T_2'}\right)\right] \qquad \textbf{(eq. 1)}.$$

where J_1 denotes the ^{1}*J*-coupling constant of the symmetrical ^{17}O site bonded to two ^{29}Si(Q^4) nuclei and *A* is a pre-factor related to the signal amplitude. For the asymmetrical siloxane (scheme **B** in Fig. **5a**), the transfer efficiency of ^{17}O{^{29}Si} *J*-HMQC experiment is proportional to

$$A[\sin^2(\pi J_1\tau)\cos^2(\pi J_2\tau)+\sin^2(\pi J_2\tau)\cos^2(\pi J_1\tau)]\left[\exp\left(-\frac{2\tau}{T_2'}\right)\right] \qquad \textbf{(eq. 2)}.$$

where J_1 and J_2 denote the ^{1}*J*-coupling constants of the asymmetrical ^{17}O site with ^{29}Si(Q^4) and ^{29}Si(Q^3) nuclei, respectively. In order to constrain the simulation of the build-up curves for the asymmetrical ^{17}O site, the ^{1}*J*-coupling constants between ^{17}O site and ^{29}Si(Q^4) nuclei were assumed to be equal in both symmetrical and asymmetrical sites. Furthermore, for the build-up curves simulation of both symmetrical and asymmetrical siloxane ^{17}O sites, we used T_2' = 65 ms, measured using Hahn-echo experiment.

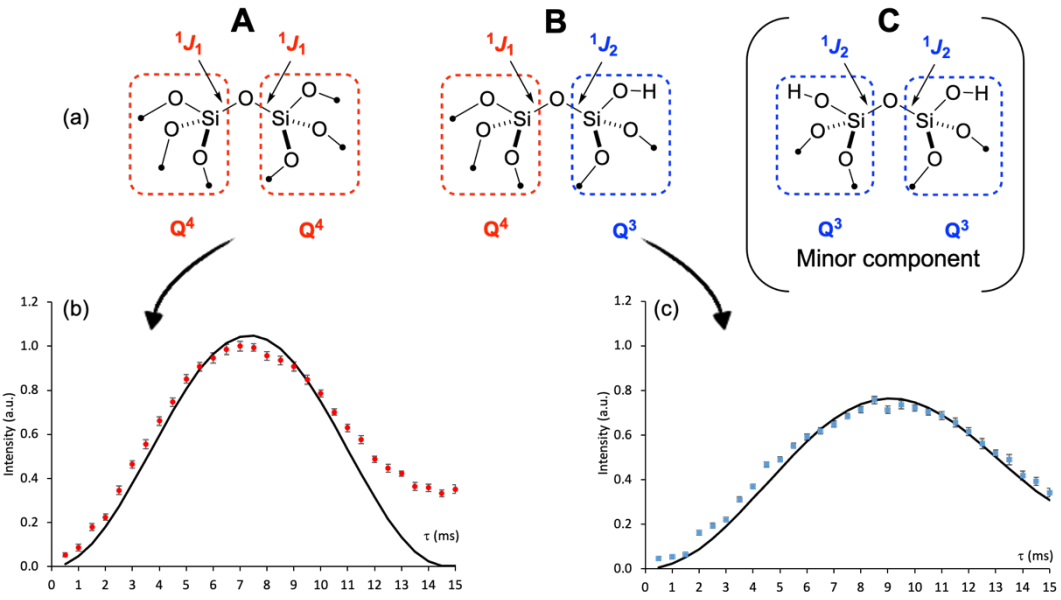

Figure 5 (a) Structure of local siloxane environments. (b,c) Build-up curves of $^{17}O\{^{29}Si\}$ DFS-*J*-HMQC-QCPMG signals at (b) 34 and (c) 22 ppm assigned to siloxane sites. The red points and the blue squares correspond to the experimental data, whereas the black lines are the simulated curves. The build-up curves were obtained by averaging 10624 transients for each of 30 t_1 increments with a recycle delay τ_{RD} = 0.5 s, leading to an experimental time of 45 h. The red and the blue points correspond to the experimental data, whereas the black lines are the simulated curves. The errors bars in the experimental curves subsume the contributions of the noise standard deviation and the error due to the nonlinear fit with DMFIT[46].

The experimental *J*-HMQC build-up curve shown in Fig. **5b** was fitted to Eq. **1**. The best-fit was obtained for J_1=$^1J_{(O\text{-}Si(Q4))}$ = 34 Hz. Using this J_1 value, the experimental *J*-HMQC build-up curve in Fig. **5c** was fitted to Eq. **2** and the best-fit J_2=$^1J_{(O\text{-}Si(Q3))}$ parameter was 23 Hz, which is lower than $^1J_{(O\text{-}Si(Q4))}$ = 34 Hz (Table 1). The significant difference between ^1J-coupling constants with Q^3 and Q^4 sites shows the influence of the second neighbours of ^{29}Si nuclei on the strength of the ^1J-coupling with siloxane ^{17}O nuclei. This effect might result from difference between $Si(Q^4)$-O-$Si(Q^4)$ and $Si(Q^3)$-O-$Si(Q^4)$ angles. The deviation between experimental data points and the simulated curves in Fig. 5b for long τ delay probably stems from a distribution of the *J*-coupling constant owing to the amorphous nature of the investigated silica. Note that the best-fit ^{17}O-^{29}Si ^1J-coupling constants are comparable to the ^{13}C-^{17}O ^1J-coupling constants measured using heteronuclear spin-echo [29] or a *J*-resolved experiment[55], which ranges from 21 to 37 Hz.

Table 1. Best-fit ^{17}O-^{29}Si ^1J-coupling constants in Hz and *A* pre-factor determined from the fit of experimental build-curves shown in Fig. 5b and c to Eqs. 1 and 2, respectively.

	Symmetrical O	**Asymmetrical O**
$^1J_{(O\text{-}Si(Q4))}$	$J_1 = 34 \pm 2$ Hz	$J_1 = 34 \pm 2$ Hz
$^1J_{(O\text{-}Si(Q3))}$		$J_2 = 23 \pm 2$ Hz
A	2.1 ± 0.2	1.4 ± 0.2

Similarly, we recorded the build-up curves of 1D ^{17}O-{^{29}Si} DFS-*D*-HMQC-QCPMG experiment. The corresponding build-up curves for symmetrical and asymmetrical siloxane sites resonating at 34 and 22 ppm are displayed in Fig. **S5**. In order to analyse these build-up curves, we simulated using SIMPSON software[40] the build-up curve of ^{17}O-{^{29}Si} *D*-HMQC-QCPMG scheme for {^{29}Si-^{17}O-^{29}Si} spin systems. The two Si···O distances were assumed to be equal for the symmetrical ^{17}O site but to differ for the asymmetrical ^{17}O site. For the symmetrical ^{17}O site, the Si···O distances were varied from 1.562 to 1.628 Å (corresponding to a dipolar coupling constant of −750 and −850 Hz respectively), whereas Si$\widehat{—O—}$Si was varied from 130° to 170° (Fig. **S6** and **S7**). The best agreement between the simulated and experimental build-up curves was obtained for $d_{\mathrm{O\ldots Si(Q4)}} = 1.628$ Å and 140° < Si$\widehat{—O—}$Si < 150°. Such value is in line with published data[56]. For the asymmetrical siloxane environment, one distance was fixed to $d_{\mathrm{O\ldots Si(Q4)}} = 1.628$ Å. The best agreement was found for an angle of Si $\widehat{—O—}$Si = 144° and a distance $d_{\mathrm{O\ldots Si(Q3)}} = 1.562$ Å which is significantly shorter than the $d_{\mathrm{O\ldots Si(Q4)}}$ distance, measured here or reported in the literature[56, 57]. The small deviations between experimental and simulated build-up curves might stem from (i) a slight distribution of ^{17}O-^{29}Si dipolar constant owing to the amorphous nature of the investigated silica, but also (ii) the dipolar coupling of ^{17}O nucleus with nearby non-covalently bonded ^{29}Si nuclei which is approximately equal to 75 Hz or the effect of ^{29}Si-^{29}Si *J*- or dipolar coupling constants, which are approximately equal to 12 and 150 Hz [58, 59].

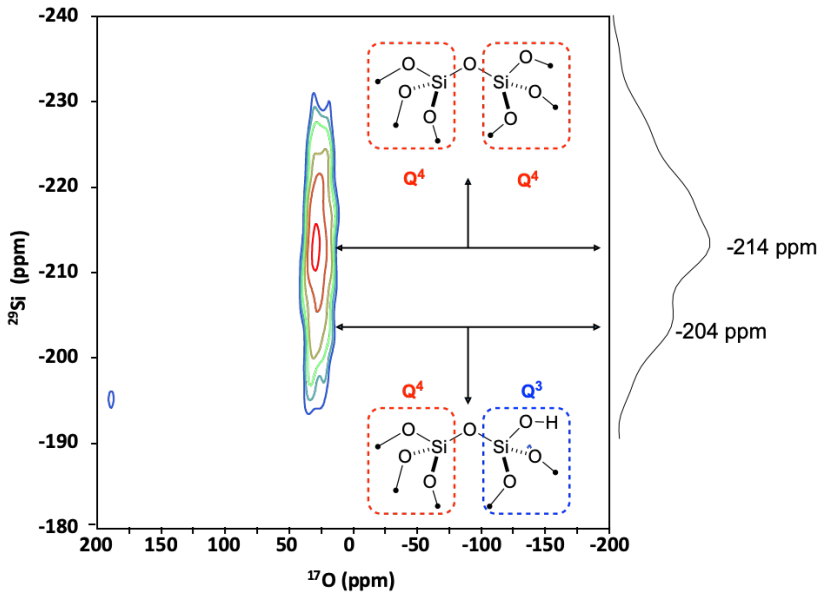

Figure 6. 2D ^{17}O{^{29}Si} 2Q-filtered DFS-*D*-HMQC-QCPMG NMR spectrum of $SiO_{2\text{-}200}$ recorded at 20 T with ν_R = 20 kHz. The projection along ^{29}Si 2Q dimension is also shown. The spectrum results from averaging 8192 and the recycle delay is 0.5 s. The recoupling time is 2 ms leading to an experimental time of 25 h.

We also carried out 2D ^{17}O-{^{29}Si} DFS-*D*-HMQC-QCPMG experiment of $SiO_{2\text{-}200}$, for which the double-quantum (2Q) coherences of ^{29}Si nuclei were selected during the indirect evolution period, t_1, using phase cycling (see Fig. **2c**). Such experiment allows selecting the signal of ^{17}O nuclei near two ^{29}Si nuclei[60]. As seen in Fig. **6**, ^{17}O signal correlate with 2Q ^{29}Si shifts of coherences at −214 and −204 ppm, ascribed

to $^{29}Si(Q^4)$-^{17}O-$^{29}Si(Q^4)$ and $^{29}Si(Q^4)$-^{17}O-$^{29}Si(Q^3)$ moieties, respectively. This result confirms the presence of these two environments near the silica surface as well as the negligible amount of $^{29}Si(Q^3)$-^{17}O-$^{29}Si(Q^3)$ sites, which would resonate near −194 ppm.

Conclusion

We have probed connectivities and proximities between ^{29}Si and ^{17}O nuclei in silica sample enriched in ^{29}Si and ^{17}O isotopes near the surface using $^{17}O\{^{29}Si\}$ *J*- and *D*-HMQC experiments at high-magnetic field. These experiments have allowed the observation of two distinct siloxane oxygen atoms, those linking two Q^4 sites and those linking Q^3 and Q^4 sites. However, the signal of silanol groups has not been detected because of their short T'_2 time constant. Furthermore, we have measured for the first time ^{17}O-^{29}Si ^1J-coupling constants for siloxane groups. We have found that the ^{17}O-^{29}Si ^1J-coupling constants are smaller for Q^4 sites than Q^3 ones and hence, that the second neighbour of ^{29}Si nuclei, H or Si atoms, affects the amplitude of ^{17}O-^{29}Si ^1J-coupling for siloxane ^{17}O nuclei. We have also shown that the simulation of the build-up of $^{17}O\{^{29}Si\}$ *D*-HMQC signals allows estimating ^{29}Si–^{17}O bond length and $Si\widehat{-O-}Si$ angle. The access to these elusive coupling constants opens new prospects for the characterization of silica surfaces, silica-supported catalysts and silicate-containing materials.

Acknowledgements

The Chevreul Institute is thanked for its help in the development of this work through the ARCHI-CM project supported by the "Ministère de l'Enseignement Supérieur de la Recherche et de l'Innovation", the region "Hauts-de-France", the ERDF program of the European Union and the "Métropole Européenne de Lille". IR-RMN and the I-Site ULNE Project OPE-2019-43 (5400 MOFFiN) are acknowledged for supporting and funding partially this work**.** We thank Franck Fayon for his help and for insightful suggestions.

Conflicts of interest

There are no conflicts to declare.

Electronic Supplementary Information

^{17}O-$\{^{29}Si\}$ DFS-HMQC-CPMG *J* and *D*-mediated NMR spectra of $SiO_{2\text{-}80}$, 1D experiments on $SiO_{2\text{-}200.}$, SIMPSON input program, details of the pulse sequences.

Notes and references

1. D. Grekov, T. Vancompernolle, M. Taoufik, L. Delevoye and R. M. Gauvin, *Chem. Soc. Rev.*, 2018, **47**, 2572-2590.
2. H. Nagashima, C. Martineau-Corcos, G. Tricot, J. Trebosc, F. Pourpoint, J. P. Amoureux and O. Lafon, *Ann. Rep. NMR Spectrosc., Vol 94*, 2018, **94**, 113-185.
3. C. Coperet, W. C. Liao, C. P. Gordon and T. C. Ong, *J. Am. Chem. Soc.*, 2017, **139**, 10588-10596.
4. S. E. Ashbrook, J. M. Griffin and K. E. Johnston, *Annu. Rev. Anal. Chem., Vol 11*, 2018, **11**, 485-508.
5. C. Bonhomme, C. Gervais and D. Laurencin, *Progr. Nucl. Magn. Reson. Spectrosc.*, 2014, **77**, 1-48.
6. D. Grekov, Y. Bouhoute, I. Del Rosal, L. Maron, M. Taoufik, R. M. Gauvin and L. Delevoye, *Phys. Chem. Chem. Phys.*, 2016, **18**, 28157-28163.
7. J. Pelletier, J. Espinas, N. Vu, S. Norsic, A. Baudouin, L. Delevoye, J. Trébosc, E. Le Roux, C. Santini, J. M. Basset, R. M. Gauvin and M. Taoufik, *Chem. Commun.*, 2011, **47**, 2979-2981.
8. A. Jystad and M. Caricato, *Chem. Mater.*, 2018, **30**, 7813-7822.
9. F. A. Perras, K. C. Boteju, Slowing, II, A. D. Sadow and M. Pruski, *Chem. Commun.*, 2018, **54**, 3472-3475.
10. F. Mauri, A. Pasquarello, B. G. Pfrommer, Y. G. Yoon and S. G. Louie, *Phys. Rev. B*, 2000, **62**, R4786-R4789.
11. T. Charpentier, P. Kroll and F. Mauri, *J. Phys. Chem. C*, 2009, **113**, 7917-7929.
12. N. M. Trease, T. M. Clark, P. J. Grandinetti, J. F. Stebbins and S. Sen, *J. Chem. Phys.*, 2017, **146**.
13. D. J. Srivastava, J. H. Baltisberger, I. Florian, F. Fayon, R. A. Shakhovoy, M. Deschamps, N. Sadiki and P. J. Grandinetti, *Phys. Rev. B*, 2018, **98**.
14. J. Keeler, *Understanding NMR Spectroscopy, 2nd Edition*, Wiley, 2010.
15. S. Berger, S. Braun and H. O. Kalinowski, *NMR Spectroscopy of the Non-Metallic Elements*, Wiley, 1997.
16. T. Terao, H. Miura and A. Saika, *J. Chem. Phys.*, 1981, **75**, 1573-1574.
17. K. W. Zilm and D. M. Grant, *J. Magn. Reson.*, 1982, **48**, 524-526.
18. T. Allman, *J. Magn. Reson.*, 1989, **83**, 637-642.
19. C. A. Fyfe, H. Gies and Y. Feng, *J. Chem. Soc.-Chem. Commun.*, 1989, 1240-1242.
20. A. Lesage, C. Auger, S. Caldarelli and L. Emsley, *J. Am. Chem. Soc.*, 1997, **119**, 7867-7868.
21. S. P. Brown, M. Perez-Torralba, D. Sanz, R. M. Claramunt and L. Emsley, *J. Am. Chem. Soc.*, 2002, **124**, 1152-1153.
22. F. A. Perras and D. L. Bryce, *J. Am. Chem. Soc.*, 2013, **135**, 12596-12599.
23. F. A. Perras and D. L. Bryce, *J. Phys. Chem. Lett.*, 2014, **5**, 4049-4054.
24. D. Franke, C. Hudalla and H. Eckert, *Solid State Nucl Magn Reson*, 1992, **1**, 33-40.
25. A. Lesage, D. Sakellariou, S. Steuernagel and L. Emsley, *J. Am. Chem. Soc.*, 1998, **120**, 13194-13201.
26. C. A. Fyfe, K. C. Wongmoon, Y. Huang and H. Grondey, *J. Am. Chem. Soc.*, 1995, **117**, 10397-10398.
27. M. Deschamps, F. Fayon, V. Montouillout and D. Massiot, *Chem. Commun.*, 2006, 1924-1925.
28. H. Nagashima, J. Trebosc, L. Calvez, F. Pourpoint, F. Mear, O. Lafon and J. P. Amoureux, *J. Magn. Reson.*, 2017, **282**, 71-82.
29. I. Hung, A. C. Uldry, J. Becker-Baldus, A. L. Webber, A. Wong, M. E. Smith, S. A. Joyce, J. R. Yates, C. J. Pickard, R. Dupree and S. P. Brown, *J. Am. Chem. Soc.*, 2009, **131**, 1820-1834.
30. S. L. Carnahan, B. J. Lampkin, P. Naik, M. P. Hanrahan, Slowing, II, B. VanVeller, G. Wu and A. J. Rossini, *J. Am. Chem. Soc.*, 2019, **141**, 441-450.
31. D. Iuga, C. Morais, Z. H. Gan, D. R. Neuville, L. Cormier and D. Massiot, *J. Am. Chem. Soc.*, 2005, **127**, 11540-11541.
32. C. Bonhomme, C. Gervais, C. Coelho, F. Pourpoint, T. Azais, L. Bonhomme-Coury, F. Babonneau, G. Jacob, M. Ferrari, D. Canet, J. R. Yates, C. J. Pickard, S. A. Joyce, F. Mauri and D. Massiot, *Magn. Reson. Chem.*, 2010, **48**, S86-S102.
33. G. P. M. Bignami, D. M. Dawson, V. R. Seymour, P. S. Wheatley, R. E. Morris and S. E. Ashbrook, *J. Am. Chem. Soc.*, 2017, **139**, 5140-5148.
34. N. Merle, J. Trébosc, A. Baudouin, I. Del Rosal, L. Maron, K. Szeto, M. Genelot, A. Mortreux, M. Taoufik, L. Delevoye and R. M. Gauvin, *J. Am. Chem. Soc.*, 2012, **134**, 9263-9275.
35. J. P. Amoureux, C. Fernandez and S. Steuernagel, *J. Magn. Reson.*, 1996, **123**, 116-118.
36. D. Iuga and A. P. M. Kentgens, *J. Magn. Reson.*, 2002, **158**, 65-72.
37. F. H. Larsen, H. J. Jakobsen, P. D. Ellis and N. C. Nielsen, *J. Phys. Chem. A*, 1997, **101**, 8597-8606.
38. S. Antonijevic and G. Bodenhausen, *Angew. Chem.-Int. Ed*, 2005, **44**, 2935-2938.
39. T. Kobayashi, J. A. DiVerdi and G. E. Maciel, *J. Phys. Chem. C*, 2008, **112**, 4315-4326.
40. M. Bak, J. T. Rasmussen and N. C. Nielsen, *J. Magn. Reson.*, 2000, **147**, 296-330.
41. M. Bak and N. C. Nielsen, *J. Magn. Reson.*, 1997, **125**, 132-139.
42. T. Charpentier, S. Ispas, M. Profeta, F. Mauri and C. J. Pickard, *Journal of Physical Chemistry B*, 2004, **108**, 4147-4161.
43. F. H. Larsen and I. Farnan, *Chem. Phys. Lett.*, 2002, **357**, 403-408.
44. D. Massiot, F. Fayon, M. Capron, I. King, S. Le Calve, B. Alonso, J. O. Durand, B. Bujoli, Z. H. Gan and G. Hoatson, *Magn. Reson. Chem.*, 2002, **40**, 70-76.
45. H. N. Kim and S. K. Lee, *Geochim. Cosmochim. Acta*, 2013, **120**, 39-64.

46. C. E. Bronnimann, R. C. Zeigler and G. E. Maciel, *J. Am. Chem. Soc.*, 1988, **110**, 2023-2026.
47. E. Lippmaa, M. Magi, A. Samoson, G. Engelhardt and A. R. Grimmer, *J. Am. Chem. Soc.*, 1980, **102**, 4889-4893.
48. T. H. Walter, G. L. Turner and E. Oldfield, *J. Magn. Reson.*, 1988, **76**, 106-120.
49. C. Fernandez, J. P. Amoureux, J. M. Chezeau, L. Delmotte and H. Kessler, *Microporous Mater.*, 1996, **6**, 331-340.
50. J. Trébosc, B. Hu, J. P. Amoureux and Z. Gan, *J. Magn. Reson.*, 2007, **186**, 220-227.
51. G. Tricot, O. Lafon, J. Trebosc, L. Delevoye, F. Mear, L. Montagne and J. P. Amoureux, *Phys. Chem. Chem. Phys.*, 2011, **13**, 16786-16794.
52. G. Tricot, J. Trébosc, F. Pourpoint, R. Gauvin and L. Delevoye, in *Ann. Rep. Nucl. Magn. Reson. Spectrosc., Vol 81*, ed. G. A. Webb, 2014, vol. 81, pp. 145-184.
53. S. Wi and L. Frydman, *J. Chem. Phys.*, 2000, **112**, 3248-3261.
54. F. A. Perras and D. L. Bryce, *J. Magn. Reson.*, 2014, **242**, 23-32.
55. G. J. Rees, S. P. Day, K. E. Barnsley, D. Iuga, J. R. Yates, J. D. Wallis and J. V. Hanna, *Phys. Chem. Chem. Phys.*, 2020, **22**, 3400-3413.
56. T. M. Clark and P. J. Grandinetti, *J. Phys.: Condens. Matter*, 2003, **15**, S2387-S2395.
57. T. M. Clark and P. J. Grandinetti, *J. Non-Cryst. Solids*, 2000, **265**, 75-82.
58. R. Challoner and C. A. McDowell, *J. Magn. Reson.*, 1992, **98**, 123-133.
59. D. J. Srivastava, P. Florian, J. H. Baltisberger and P. J. Grandinetti, *Phys. Chem. Chem. Phys.*, 2018, **20**, 562-571.
60. C. Martineau, F. Fayon, C. Legein, J. Y. Buzare, G. Silly and D. Massiot, *Chem. Commun.*, 2007, 2720-2722.